IABSE Symposium 2025
Environmentally Friendly Technologies and Structures - Focusing on Sustainable Approaches
May 18-21, 2025 | Tokyo, Japan

Flexural strength and behaviour of cold rolled purlins with complex longitudinal stiffeners

Van Bac Nguyen

University of Derby, Derby, DE22 3AW, United Kingdom

Iman Hajirasouliha

The University of Sheffield, Sheffield, S1 3JD, United Kingdom

Martin English

Hadley Industries plc, Smethwick, B66 2PA, United Kingdom

Contact: vb.nguyen@derby.ac.uk

Abstract

This paper presents the flexural strength and behaviour of cold rolled channel and zed steel purlins with complex longitudinal web and flange stiffeners. The material properties at the section's flat parts, corners, and stiffeners are obtained from tensile tests. A series of four-point beam bending tests is carried out to determine the buckling and ultimate bending capacities of these sections. Nonlinear Finite Element analysis (FEA) is developed to model the flexural strength of the purlins and validated against the experimental tests. True stress-strain data for materials due to cold working at different regions of the sections are incorporated into nonlinear analyses. Based on the validated FEA results for different sectional shapes and thicknesses, design formulae for determining flexural strength of purlin sections with complex stiffeners are developed.

Keywords: Cold rolled sections; purlins; cold working; channel section; zed section; buckling; ultimate strength; tensile test; four-point bending test; Finite Element analysis.

1 Introduction

In building construction, cold-rolled purlin sections are typically produced in standard channel and zed profiles. These sections are made up of plate elements for the web and flanges, which generally have a high width-to-thickness ratio. As a result, they are susceptible to buckling (local or distortional buckling), and their buckling modes primarily determine the failure behaviour of cold-rolled sections. A main method to enhance the buckling strength of cold-rolled sections is by incorporating longitudinal stiffeners on the web or flange. These stiffeners divide the flat elements of the web and flange into sub-elements, which significantly increases the buckling load of sections (due to the reduced width-to-thickness ratio of the sub-elements). Stiffeners can be categorised into "standard" stiffeners, such as symmetrical angles as shown in pre-qualified profiles in codes of

practice [1-3], and "complex" stiffeners, like unsymmetrical angles with multiple curved bends or semi-circular shapes [4], as shown in Figure 1.

Practical design guidelines for designing cold formed sections the sections with standard stiffeners are generally provided in the codes of practice of various countries, including the European Standard [1], North American Specification [2], and Australian/New Zealand Standard [3] but there has been limited guidance for sections with complex stiffeners rather than standard ones [4-5]. The Finite Element analysis (FEA) has been extensively used in the analysis and design of cold-formed steel structures; however, there have been limited studies on cold-formed steel sections with stiffeners subjected to bending. Study [6] employed FEA to better understand the behaviour of intermediately stiffened elements of hat sections under pure bending. Recent research on the buckling and ultimate strengths of channel and zed sections with stiffeners, utilizing FEA and optimisation techniques, has been presented in [7-8].

Complex stiffeners have been incorporated into purlin sections, with the aim of improving the flexural strength of channel and zed sections [8,9]. These sections have a considerably improved strength to weight ratio considerably by using the web stiffener types of unsymmetrical angles as shown in Fig. 1. However, the design of these sections using design codes such as the European standard Eurocode 3 [1], is very complicated and impractical in calculating the effective section properties and buckling modes such as distortional buckling due to the complex folded-in stiffeners. In addition, during the cold-rolled forming process, varying levels of cold working or plastic deformation occur within the material, leading to changes in the mechanical properties of the original coil. However, there have not been studies on effects of cold working on the flexural strength of beam sections with complex stiffeners.

In this paper, nonlinear FEA models were then developed for channel and zed beams subjected to four-point bending tests and were validated against test data. True material properties at section corners and stiffeners were obtained from tensile testing. Based on the validated Finite Element results for different sectional shapes and thicknesses, standard design formulae for determining buckling and ultimate loads of channel and zed sections were developed.

2 Experimental test programme

2.1 Bending tests

Typical cold-rolled cross sections of the test purlins are shown in Figure 1 where sections are industrial channel and zed sections namely UltraBEAM^{TM}2 and UltraZED^{TM}2, respectively, developed by Hadley Industries plc. For the section depths less than 200 mm, the load centre span is 900 mm; for the section depths greater than 200 mm, the load centre span is 1030 mm. Measured test section dimensions are given in Table 1 for channel sections and Table 2 for zed sections. The specimens were labelled, a channel specimen label starts with C whilst a zed specimen starts with Z. For example, a specimen labelled as C-W145T1.2 is described as follows: C: Channel specimen; W: Web, 145: Nominal web height or beam depth (mm); T: Thickness, 1.2: Nominal plate thickness (mm). In this test programme, channel and zed specimens with depths of 145 mm and 200 mm, and thicknesses of 1.20 mm and 2.00 mm were tested. Other specimens were test in the previous test programme [4].

The standard setup is illustrated in Figure 2, which depicts the arrangement of a zed section. The beam sections were paired and laterally restrained using 45x45 mm steel angles at 500 mm intervals. However, there were no restraints on the upper part of the sections in the loading span at the mid-span. A calibrated test rig with a 200-kN capacity hydraulic actuator was utilized for the tests. The actuator applied the load via a rigid I-beam onto the beam specimens at two points spaced the load centre apart. Four strain gauges were mounted at the mid-span of each section, positioned around the perimeter outside the specimen's cross-section, near the flange-web junctions, and at the centres of the flanges. LVDTs were placed at mid-span length and at supports to monitor any vertical displacement. Rotation dial gauges were placed at mid-span and support positions to measure the

rotation of the beams. A displacement-controlled loading scheme with a rate of 1 mm/min was applied throughout the tests. The specimens were loaded to failure, with the tests ceasing at approximately 70% of the ultimate load.

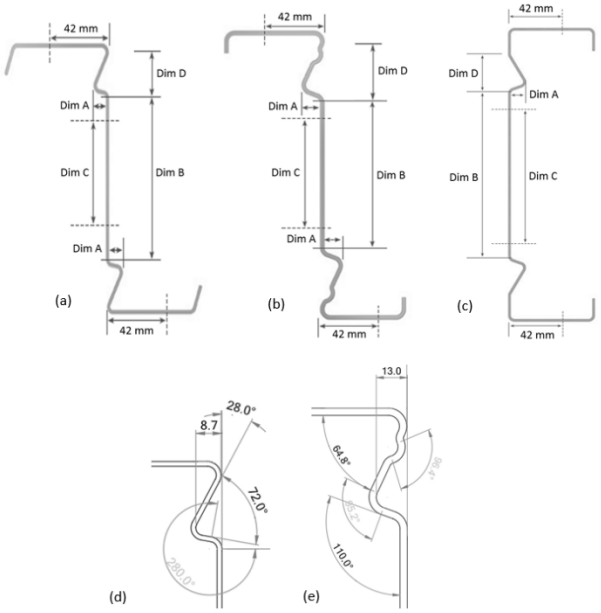

Figure 1. Cross sections (a) zed 145-170 mm deep sections, (b) zed 200-305 mm deep sections, (c) channel 145-305 mm deep sections, (d) unsymmetrical stiffeners, and (e) unsymmetrical stiffeners with additional bends.

2.2 Tensile tests

The material properties of the flat parts, corners, and stiffeners were determined through tensile tests. The locations of the extracted specimens for each type of beam section are illustrated in Figure 3, starting with the type (web, flange, and corner), followed by their positions, labelled as a, b, c. Three flat specimens were extracted from the centreline of the web, and three from the centreline of the flange. The flat specimens had a parallel length of 75 mm and a width of 12.50 mm, while the curved specimens had a parallel length of 75 mm with varying widths, ranging from 3.5 to 12.5 mm, depending on their positions and the dimensions of the cross-sections.

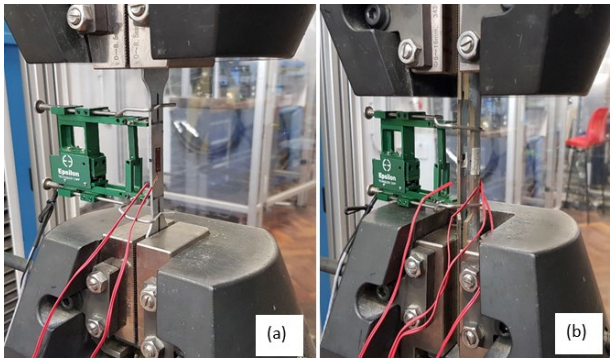

Figure 4. Typical tensile test setup (a) flat specimens and (b) curved specimens.

3 Finite Element Analysis

FE modelling was performed using ANSYS (Version 2023, ANSYS, Inc.) to model the four-point bending test of the channel and zed sections. The FE model setup including point load locations and boundary conditions is illustrated in Figure 5 where only half of the test system was simulated due to symmetry. The bracings were modelled using tie nodes at the symmetry plan that were rigidly connected to nodes from the top or bottom flanges, and they were constrained to prevent from movement against the transverse direction. The connections of support cleats attached to the web of the section at supports and loading points were also modelled by rigid connections between reference nodes (at centre of support) and nodes at screw positions. Shell elements SHELL181 which has 4-noded quadrilateral, reduced integration, were selected. The material properties for flat parts, section and stiffener's corners obtained from tensile tests were assigned in these regions of the channel and zed sections in the FE models. True stress-strain data obtained from tensile tests for materials at different regions are incorporated into nonlinear FEA.

4 Test results and discussion

4.1 Tensile tests

Table 3 presents the measured material properties for both flat and curved specimens for typical flat specimens and pairs of curved specimens from

sections C-W145T1.2 and Z-W145T1.2. In this table, f_y represents the 0.2% proof stress, f_u denotes the ultimate tensile strength, and ε_f is the elongation after fracture. For flat specimens, the average result of three repeated tests a, b, c was presented; for corner specimens, the average result of two repeated tests a, b was presented.

Figure 6 illustrates the static stress-strain curves shown as conventional engineering values. For the channel section, the yield and tensile strengths of the curved specimens increased by 7–12% and 4–10%, respectively, compared to flat specimens. Similarly, for the zed section, yield and tensile strengths of the curved specimens increased by 16–20% and 16–18%, respectively.

Table 3. Measured material properties of tensile specimen of channel and zed sections.

Section	Type	Region	f_y (N/mm^2)	f_u (N/mm^2)	ε_f (%)
Channel C-W145T1.2	Flat	Flange	488.72	562.88	17
		Web	500.46	568.00	16
	Corner	Position 1	522.53	621.03	6
		Position 2	554.29	618.06	7
		Position 3	549.98	585.48	6
Zed Z-W145T1.2	Flat	Flange	467.32	545.09	23
		Web	460.21	536.36	23
	Corner	Position 1	549.53	636.60	11
		Position 2	539.21	638.11	13
		Position 3	556.30	626.36	10

Table 1. Measured test section geometries and dimensions for channel sections.

Channel sections				Flange		Dim A	Dim D	Dim B	Second Moment	Section modulus
Section Reference	Thickness mm	Depth mm	Radius mm	Width mm	Lip mm	mm	mm	mm	Major axis mm^{4}x10^4	Major axis mm^{3}x10^3
C-W145T1.2	1.23	145.04	2.30	63.07	16.05	9.00	20.00	75.00	121.54	16.76
C-W145T1.4	1.40	145.02	2.10	62.98	16.01	9.00	20.00	75.00	141.10	19.46
C-W145T2.0	1.99	145.01	1.50	63.05	16.01	9.00	20.00	75.00	198.64	27.40
C-W170T1.2	1.20	170.05	2.30	63.01	16.05	9.00	20.00	100.00	176.09	20.72
C-W170T1.5	1.50	169.80	2.00	62.99	15.94	9.00	20.00	100.00	218.66	25.72
C-W170T1.6	1.60	170.10	2.00	63.10	16.05	9.00	20.00	100.00	232.27	27.31
C-W170T2.0	2.01	170.00	1.50	63.04	15.98	9.00	20.00	100.00	288.34	33.92
C-W200T1.2	1.20	200.01	2.20	63.03	18.02	12.50	30.00	125.00	258.23	21.29
C-W200T2.0	2.01	199.05	1.50	63.05	18.01	12.50	30.00	125.00	423.61	34.18
C-W255T1.4	1.40	254.90	3.00	75.00	19.03	12.50	30.00	155.00	742.64	58.25
C-W255T2.3	2.32	255.02	2.10	75.06	19.02	12.50	30.00	155.00	820.21	64.33
C-W255T3.0	2.98	255.01	1.40	74.97	19.07	12.50	30.00	155.00	1009.89	79.21

Table 2. Measured test section geometries and dimensions for zed sections.

Zed Sections				Top flange		Bottom flange		Dim A	Dim D	Dim B	Second moment	Section modulus
Section Reference	Thickness mm	Depth mm	Radius mm	Width mm	Lip mm	Width mm	Lip mm	mm	mm	mm	Major axis mm^{4}x10^4	Major axis mm^{3}x10^3
Z-W145T1.2	1.25	145.07	2.70	67.00	15.02	61.03	13.89	10.00	25.00	90.00	126.95	17.18
Z-W145T1.5	1.55	145.01	2.60	67.04	15.03	61.00	13.92	10.00	25.00	90.00	157.43	21.29
Z-W145T2.0	2.00	145.00	2.30	66.95	15.05	60.96	13.94	10.00	25.00	90.00	207.14	28.02
Z-W170T1.6	1.60	170.00	2.00	69.08	14.98	61.01	13.40	10.00	25.00	115.00	240.40	28.28
Z-W200T1.2	1.22	199.70	5.40	70.03	14.92	60.08	13.05	15.00	42.50	100.00	257.32	25.06
Z-W200T1.8	1.77	200.03	5.10	70.01	15.05	59.97	13.07	15.00	42.50	100.00	382.70	37.26
Z-W200T2.0	2.01	200.02	5.00	69.85	15.04	60.82	13.04	15.00	42.50	100.00	423.15	53.64
Z-W200T2.5	2.42	200.06	4.75	69.40	15.04	60.02	12.92	15.00	42.50	100.00	522.47	50.86
Z-W255T1.3	1.28	255.00	5.35	69.70	14.97	59.91	13.00	13.00	42.50	155.00	500.84	38.38
Z-W255T1.8	1.82	255.02	5.10	70.06	14.91	59.96	13.04	13.00	42.50	155.00	689.19	52.58
Z-W255T2.5	2.47	254.80	4.75	70.02	15.02	60.01	12.95	13.00	42.50	155.00	938.99	71.93

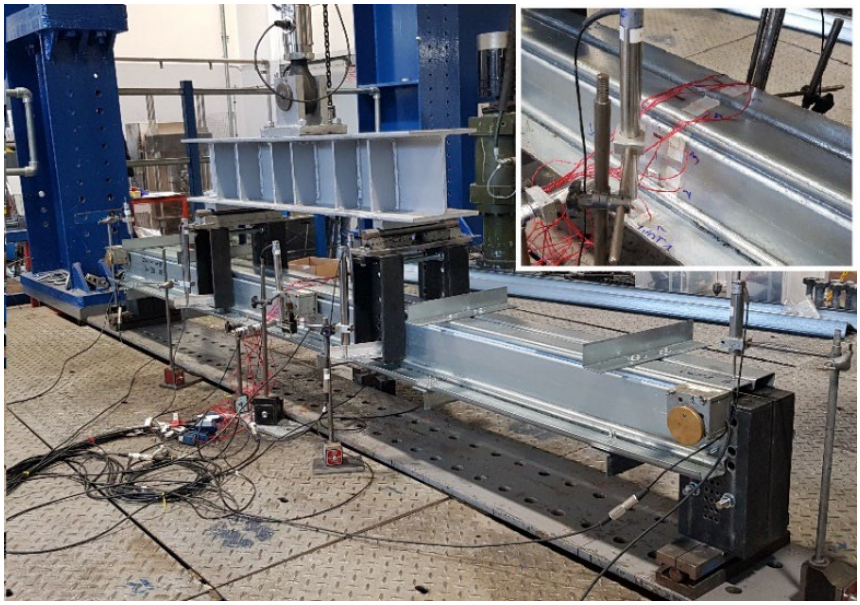

Figure 2. Four-point bending test setup, showing zed sections and strain gauge arrangement (in box).

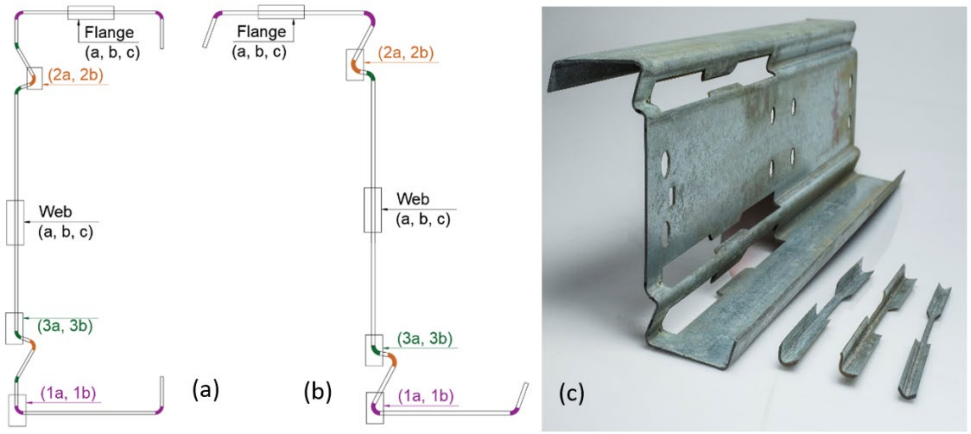

Figure 3. Locations of extracted tensile specimens (a) channel cross section, (b) zed cross section, and (c) typical curved specimens wired cutting from the section Z-W145T1.2 and specimens extracted from curved locations 1, 2, and 3.

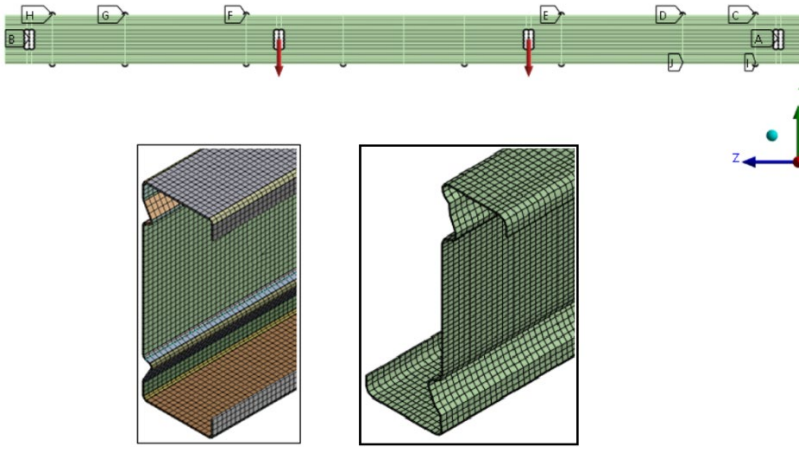

Figure 5. FE four-point bending test setup including boundary conditions and a closer view of the mesh of a channel and zed beams.

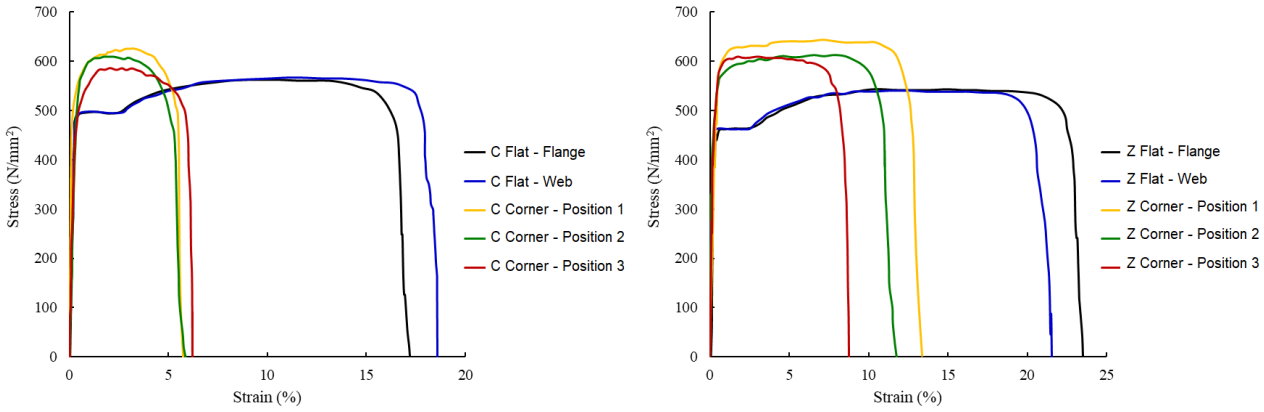

Figure 6. Engineering stress–strain relationships of flat and corner specimens for (a) channel section C-W145T1.2, and (b) zed section Z-W145T1.2.

Table 5. FE results and comparison of moment capacities and test results. The bold texts present specimens of the test programme in this paper while the rest are specimens from the previous test programme [4].

Specimens	Test	FEA without cold working effect			Comparison	FEA with cold working effect			Comparison
	M_{u_EXP} (kNm)	M_{crd} (kNm)	M_{u_FEA} (kNm)	M_y (kNm)	M_{u_EXP} / M_{u_FEA} (kNm)	M_{crdc} (kNm)	M_{uc_FEA} (kNm)	M_{yc} (kNm)	M_{u_EXP} / M_{uc_FEA} (kNm)
(1)	(2)	(3)	(4)	(5)	(6) = (2)/(4)	(7)	(8)	(9)	(10) = (2)/(8)
Channel									
C-W145T1.2	**5.15**	**5.12**	**5.38**	**8.27**	**0.96**	**5.14**	**5.62**	**8.86**	**0.92**
C-W145T2.0	**12.46**	**14.75**	**10.85**	**13.46**	**1.15**	**14.75**	**11.82**	**15.38**	**1.05**
C-W200T1.2	**8.82**	**9.07**	**10.67**	**17.68**	**0.83**	**9.07**	**11.28**	**20.14**	**0.78**
C-W200T2.0	**16.66**	**26.52**	**19.36**	**23.93**	**0.86**	**26.52**	**20.41**	**26.72**	**0.82**
C-W145T1.2	5.97	5.30	6.19	10.19	0.96	5.33	6.71	11.64	0.89
C-W145T1.4	6.54	7.06	6.60	9.41	0.99	7.09	7.02	10.73	0.93
C-W145T2.0	11.24	14.97	10.77	13.20	1.04	15.00	11.27	15.02	1.00
C-W170T1.2	6.63	6.15	7.41	12.47	0.89	6.18	7.61	13.02	0.87
C-W170T1.5	8.43	9.30	9.47	14.27	0.89	9.32	9.54	14.40	0.88
C-W170T1.6	9.08	10.57	9.92	14.17	0.92	10.61	10.58	10.58	0.86
C-W170T2.0	12.75	16.30	13.18	17.25	0.97	16.35	13.90	19.94	0.92
C-W255T1.5	13.21	14.23	13.46	19.36	0.98	15.35	14.32	21.81	0.92
C-W255T2.3	23.82	34.58	24.86	30.48	0.96	34.73	27.60	39.38	0.86
C-W255T3.0	40.09	62.93	37.83	42.43	1.06	61.82	40.95	50.85	0.98
Zed									
Z-W145T1.2	**5.49**	**25.08**	**5.87**	**8.05**	**0.94**	**28.64**	**5.94**	**9.15**	**0.92**
Z-W145T2.0	**13.19**	**73.54**	**13.41**	**13.70**	**0.98**	**73.54**	**14.15**	**14.15**	**0.93**
Z-W200T1.2	**9.82**	**29.92**	**10.41**	**10.41**	**0.94**	**29.92**	**11.16**	**11.16**	**0.88**
Z-W200T2.0	**18.16**	**85.26**	**19.37**	**29.85**	**0.94**	**85.26**	**21.44**	**21.44**	**0.85**
Z-W145T1.2	7.29	25.29	7.53	7.53	0.97	25.32	8.21	8.21	0.89
Z-W145T1.5	9.50	40.21	9.97	9.97	0.95	40.20	10.68	10.68	0.89
Z-W145T2.0	12.35	73.54	13.68	13.68	0.90	75.57	14.92	14.92	0.83
Z-W170T1.6	12.35	41.72	14.70	13.68	0.84	41.65	15.84	15.84	0.78
Z-W200T1.2	14.80	29.72	14.80	15.31	1.00	29.92	15.02	15.59	0.99
Z-W200T1.8	17.19	68.81	20.56	20.56	0.84	68.87	21.20	21.20	0.81
Z-W200T2.5	22.20	135.65	23.84	23.83	0.93	135.55	25.50	25.50	0.87
Z-W255T1.3	16.50	29.98	16.93	18.46	0.97	29.81	17.97	20.17	0.92
Z-W255T1.8	25.18	58.90	26.09	26.09	0.97	59.00	27.87	28.43	0.90
Z-W255T2.5	31.98	115.15	32.86	32.86	0.97	115.14	35.49	39.43	0.90

4.2 FE modelling and validation

Table 5 summarizes the comparison of ultimate moment capacities for beams. M_{u_EXP} is the experimental result. M_{crd} is the critical distortional buckling value. M_y , M_{u_FEA} are the section's yield and ultimate bending moment capacities while M_{yc} , M_{uc_FEA} are the section's yield and ultimate bending moment capacities with consideration of the true material properties at section corners and stiffeners affected by cold working.

The FEA results showed excellent agreement with the experimental values for ultimate moment capacities for tested specimens in this test programme (the first 4 channel and zed specimens shown in Table 5). Additionally, a strong correlation between the experimental results and the FE simulation models is evident in the load-displacement curves presented in Figures 7 and 8.

4.3 FE modelling and validation

Table 5 summarizes the comparison of ultimate moment capacities for beams. M_{u_EXP} is the experimental result. M_{crd} is the critical distortional buckling value. M_y , M_{u_FEA} are the section's yield and ultimate bending moment capacities while M_{yc} , M_{uc_FEA} are the section's yield and ultimate bending moment capacities with consideration of the true material properties at section corners and stiffeners affected by cold working.

The FEA results showed excellent agreement with the experimental values for ultimate moment capacities for tested specimens in this test programme (the first 4 channel and zed specimens shown in Table 5). Additionally, a strong correlation between the experimental results and the FE simulation models is evident in the load-displacement curves presented in Figures 7 and 8. The FE models accurately captured the distortional buckling failure mode, as reflected in the deformed shapes of the channel section in Figure 7(b) and the zed section in Figure 8(b).

5 Design of cold-rolled channel and zed purlin sections

The verified FEA models developed in Section 4 were used for analyses of all channel and zed specimens in the test programmes as shown in Tables 1 and 2. Table 5 summarizes all FEA results of ultimate bending moment capacities and comparisons to experimental results are shown in column (6) and (10) for the cases without and with the cold working effect, effectively.

Comparison of the FEA results with experimental test results shows a minimum variation of 1% up to a maximum of 15% for channel sections, and 3% to 16% for zed sections. The average variation is 8% and 10% for all data of channel and zed sections, respectively, with the FE giving fewer conservative results in 2/20 cases. In addition, the modes of failure observed during experimental tests were similar with those obtained from the FEA calculations. These show a very good agreement between test and FEA values. Many zed specimens failed at yield bending moment, so their cross sections were fully effective or under full section failure mode whilst beams with depths of 145 mm did not show buckling failure clearly, so they were also defined as full section failure.

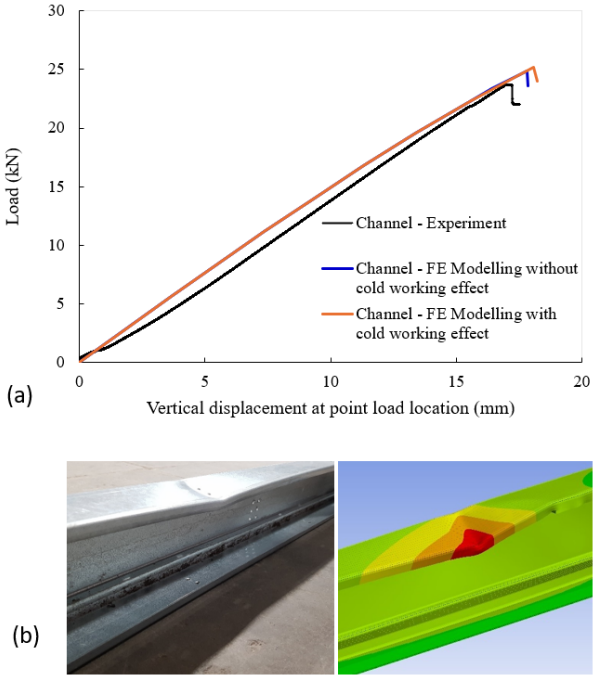

Figure 7. Experimental and FEA modelling results for channel section C-W145T1.2 (a) typical load-displacement curves, and (b) deformed shapes at failure from experiment and FE modelling.

Including the cold working effect in the sections' corners and stiffeners' bends could lead to noticeable enhancement in the ultimate moment capacities of some channel and zed sections, as indicated in Table 5. The maximum percentage of increase in the ultimate moment capacities with the cold working effect was up to 10%, confirming

that the influence of the cold working effect could be significant. There were insignificant effects for the few cases where the sections were more prone to distortional buckling (the sections with higher distortional buckling slenderness gained less strength benefit from the cold working effect).

Expressions of the normalised moment capacity M_u/M_y versus the slenderness $(M_y/M_{crd})^{0.5}$, or M_{uc}/M_{yc} versus the slenderness $(M_{yc}/M_{crd})^{0.5}$ when the cold working effect is considered, were established by power function fits using the least square method, as illustrated in Figures 9 and 10; they are used as design formulae for determining the ultimate moment capacity of channel and zed sections with complex stiffeners.

The regression curves and the FEA results were obtained with a very good agreement for the ultimate moment capacity data (the correlation coefficient r^2 = 0.70-0.99) for channel sections. However, the curves for zed sections were almost flat as most of zed sections reached full section strength (no distortional buckling occurred); therefore, the correlation coefficient r^2 is almost zero).

6 Conclusions

The experimental test, analysis design by FEA for the channel and zed purlins with complex web longitudinal stiffeners were studied. Four-point bending tests and tensile tests of materials at flat, corner and stiffener regions of these beams were conducted. Nonlinear buckling Finite Element models were developed for the bending tests and validated against the test results.

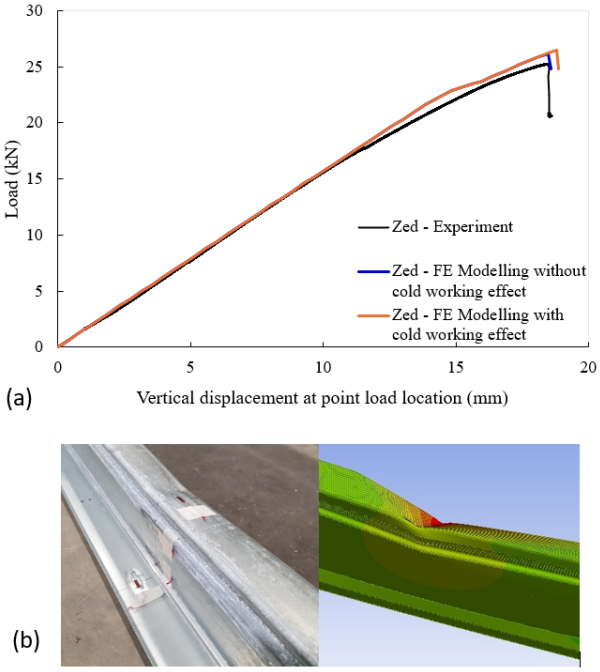

Figure 8. Experimental and FEA modelling results for zed section Z-W145T1.2 (a) typical load-displacement curves, and (b) deformed shapes at failure from experiment and FE modelling.

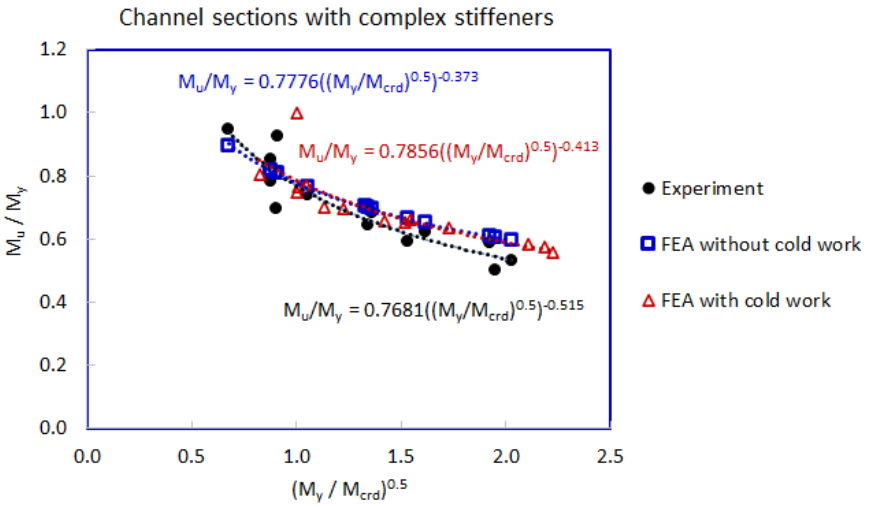

Figure 9. Graph of M_u/M_y versus $(M_y/M_{crd})^{0.5}$ and regression curves for channel sections for test results (r^2 = 0.85), FEA without cold working results (r^2 = 0.99), and FEA with cold working results (r^2 = 0.70).

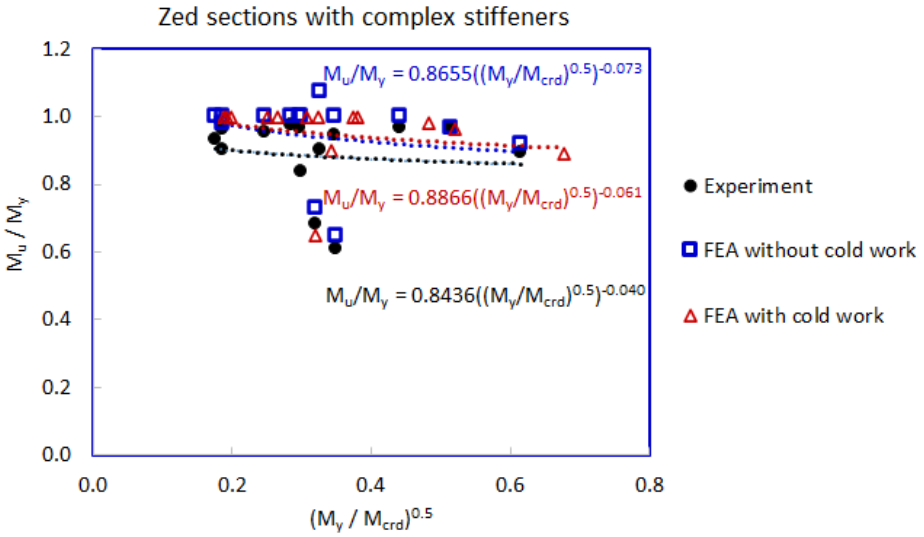

Figure 10. Graph of M_u/M_y versus $(M_y/M_{crd})^{0.5}$ and regression curves for zed sections for test results (r^2 = 0.01), FEA without cold working results (r^2 = 0.04), and FEA with cold working results (r^2 = 0.05).

Comparison of the FEA results with physical test results shows an average variation of 8% for the channel sections and 10% for the zed sections, with the FEA giving conservative results in 2/20 cases. This shows that the nominal moment capacities predicted using the FEA are very comparable with test results for the channel and zed purlins subjected to bending. It was observed that the distortional buckling dominated the behaviour and failure mode of all the channel sections whilst it occurred only in few zed sections; most of zed sections behaved elastically in full strength without buckling. Significant enhancement in the ultimate moment capacities of some channel and zed sections could be obtained (up to 10%) when the cold working effect in the sections' corners and stiffeners' bends were considered.

7 References

[1] E. CEN, 1-3 Eurocode 3: Design of steel structures-Part 1-3: General rules-Supplementary rules for cold-formed members and sheeting. European Committee for Standardization, Brussels; 2006.

[2] AISI S100-16 North American specification for the design of cold-formed steel structural members. Washington, DC; 2016.

[3] AS/NZS 4600:2005 Cold-Formed Steel Structures. Standards Australia/ Standards New Zealand; 2005.

[4] Nguyen V.B. et al. Design of new cold rolled purlins by experimental testing and Direct Strength Method. *Thin-Walled Structures*. 2017; 118: 105-112.

[5] Ye J. et al. Development of more efficient cold-formed steel channel sections in bending. *Thin-Walled Structures*. 2016; 101: 1-13.

[6] Qadir S.J., Nguyen V.B., Hajirasouliha I., Cartwright B., and English M.A. Optimal design of cold roll formed steel channel sections under bending considering both geometry and cold work effects. *Thin-Walled Structures*. 2021; 157, 107020.

[7] Schafer B. and Peköz T. The behavior and design of longitudinally stiffened thin-walled compression elements. *Thin-walled structures*. 1997; 27: 65-78.

[8] Qadir S.J., Nguyen V.B., Hajirasouliha I., Ceranic B., Tracada E., and English M.A. Shape optimisation of cold roll formed sections considering effects of cold working. *Thin-Walled Structures*. 2022; 170, 108576.